**CAMBRIDGE
UNIVERSITY PRESS**

Sub-terahertz propagation characteristics up to 150 GHz for 6G mobile communication systems

Minoru Inomata[1] , Wataru Yamada[1], Nobuaki Kuno[1], Motoharu Sasaki[1], Koshiro Kitao[2], Mitsuki Nakamura[2], Takahiro Tomie[2] and Yasuhiro Oda[2]

[1]NTT Access Network Service Systems Laboratories, NTT Corporation, 1-1 Hikarino-oka, Yokosuka-shi, Kanagawa, Japan and [2]6G-IOWN Promotion Department, NTT DOCOMO, INC., 3-6 Hikarino-oka, Yokosuka-shi, Kanagawa, Japan

Abstract

Extreme-high-speed communication exceeding 100 Gbps is one requirement for 6G. To satisfy extreme-high-speed-communication, one solution is to utilize terahertz bands above 100 GHz. To determine the new radio-interface technologies and service frequency bands for 6G, terahertz propagation characteristics above 100 GHz need to be understood. In this paper, we introduce our new radio-network topology for 6G and then show the frequency dependency of key propagation phenomena such as the characteristics of path loss in an urban environment, human blockage, and scattering from a rough building surface up to 150 GHz. Human blockage loss increases and the scattering is more diffused as the frequency increases. In the path-loss characteristics, it was found that path-loss frequency dependency is stronger than that given by conventional path-loss model because of scattering effects from a rough building surface.

Introduction

In 2020, fifth generation (5G) mobile communication systems have been rolled out worldwide. 5G New Radio supports millimeter wave (mmW) bands up to 52.6 GHz, and an extension to 71 GHz is being examined for future releases [1]. In the 2030s, the new market value created by 5G is expected to be enlarged through next-generation 6G. Extreme-high-speed communication exceeding 100 Gbps is one requirement for 6G [2]. As one solution, utilization of the terahertz (THz) bands above 100 GHz has been considered all over the world because a remarkably wider frequency bandwidth can be utilized than even in 5G [1–3]. We note that the formal definition of the THz bands is from 300 GHz to 3 THz, but, in this paper, we call the 100–300 GHz bands sub-THz bands. At WRC-19, the 275–450 GHz bands were newly considered frequency bands for use in land mobile and fixed services [1]. In addition, the US Federal Communications Commission (FCC) recommends 95 GHz to 3 THz bands for 6G [3]. However, specific new radio-interface technologies and service frequency bands have yet to be determined because propagation characteristics above 71 GHz have not been studied sufficiently. In the mmW bands for 5G, the measurement results show an increased frequency dependency of path loss and an increased number of occurrences of some blockage due to humans and small structures [4–7]. Although 5G channel models have been standardized in ITU-R M.2412, they have been constructed by using measurement frequency bands mainly below 71 GHz [5–7]. For the THz bands for 6G, these phenomena are more sensitive and introduce increased dependence on frequency. Furthermore, the new propagation phenomenon, which is not considered by 5G channel models, may be required to exploit the THz bands. Specifically, in the case of scattering from a rough surface, the higher the frequency, the larger the scattering power and the lower the reflection power, so it is necessary to clarify the scattering effects on channel characteristics in the THz bands. Therefore, for the development of 6G mobile communication systems using new frequency bands above 100 GHz, it is important to clarify the THz propagation phenomena and develop the channel models for the THz bands.

In this paper, we briefly introduce our new radio-network topology concept for 6G and key propagation phenomena that should be clarified in the sub-THz bands to develop channel models. When using our new radio-network topology for 6G in an urban microcell (UMi), which is the main scenario of mobile communication systems, designing the new radio-network topology with high accuracy requires the key propagation phenomena to be clarified, such as the path-loss characteristics, human blockage, and scattering effects from rough building surfaces, for the sub-THz bands are needed to be clarified. Therefore, we investigate the frequency dependency of path-loss characteristics, human blockage, and scattering effects from rough building surfaces up to 150 GHz bands [8].

Key propagation phenomena affecting sub-THz channel characteristics

Figure 1 shows a new radio-network topology concept [2]. In the sub-THz bands, the path loss becomes larger than that in the existing mmW bands of 5G. Therefore, when
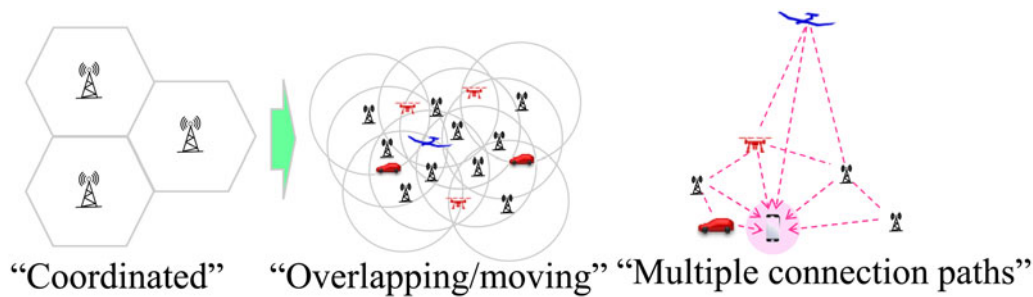
Fig. 1. Evolution of radio-network topology for 6G.
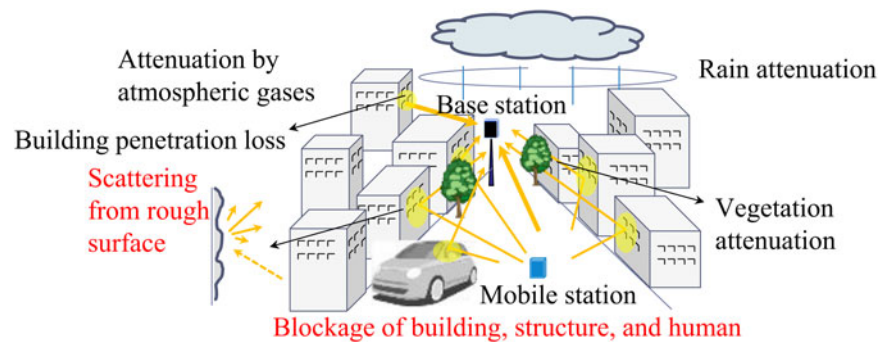
Fig. 2. Key propagation phenomena for sub-THz bands.

extreme-high-speed and high-reliability communication are pursued, it is ideal to communicate at as close a distance and in as unobstructed a path as possible. Cellular networks were constructed with a hexagonal cell layout in which base stations' positions are coordinated. However, to increase the unobstructed and close paths in the sub-THz bands, a spatially overlapping topology needs to be constructed. To efficiently actualize a distributed network in the space domain, various solutions need to be investigated such as integrated access and backhaul [9], intelligent reflecting surface [10], and cooperation with non-terrestrial networks. In addition, when using the same frequency band in the same space, inter-cell interference occurs. Therefore, it is essential to clarify path-loss and channel characteristics based on the sub-THz propagation phenomena and evaluate the performance of those techniques for a new radio-network topology.

To design the new radio-network topology with high accuracy, it is important to clarify the propagation phenomena and develop channel models on the basis of use cases for 6G. Figure 2 shows the key propagation phenomena that affect channel characteristics for the sub-THz bands in an UMi. ITU-R M.2412 proposed models that can calculate path loss that building shadowing and human blockage is considered and the building penetration loss in accordance with the mixing ratio of building materials; however, the models are constructed by using measurement frequency bands below 71 GHz [4–7]. Also, a representative atmospheric attenuation model up to 1 THz was reported in ITU-R P.676 [11], and rain attenuation model up to 1 THz was reported in ITU-R P.838 [12]. In addition, vegetation attenuation up to 30 GHz was reported in ITU-R P.833 [13], and scattering from rough surfaces was mainly investigated below 71 GHz [5]. As previously mentioned, a number of studies have been conducted on the channel characteristics of the THz bands, but the characteristics above the 71 GHz band for 6G have not been sufficiently studied. Therefore, in this paper, we

Table 1. Measurement parameters

Frequency	0.8, 2.2, 3.4, 4.7, 8.5, 27.9, 37.1, 66.5, 97.5, 150 GHz
Signal	Continuous wave (CW)
Tx/Rx antenna	Horn antenna at 150 GHz, omni-directional antenna at 0.8, 2.2, 3.4, 4.7, 8.5, 27.9, 37.1, 66.5, and 97.5 GHz
Tx/Rx antenna height	Approximately 1.8 m

investigate the frequency dependency of human blockage, scattering from rough building surfaces and characteristics of path loss in an UMi from microwave bands to sub-THz bands to evaluate 6G system performances.

Frequency dependency of key phenomena

Human blockage

Human blockage loss was measured from 0.8 to 150 GHz bands to clarify the frequency dependency. We selected 0.8, 2.2, 3.4, 4.7, 27.9, 37.1, and 66.5 GHz to cover the frequency bands assigned to mobile communication systems up to 5G and 8.5, 97.5, and 150 GHz in 7–10 GHz, and sub-THz bands agreed with candidate frequency bands for 6G. The measurement parameters are shown in Table 1. Figure 3 shows the measurement setup and results. In Figs 3(a) and 3(b), in the measurement, the distance between the antenna and the human body was set to about 2 m, and the antenna height was set to 1.8 m corresponding to human chest height. The human body was moved at intervals of 0.05 m. The Tx and Rx antenna are an omni-directional antenna with an antenna gain of 2.5 dBi at 0.8 GHz, 2.7 dBi at 2.2 GHz, 2.3 dBi at 3.4 GHz, 2.5 dBi at 4.7 GHz, 2.0 dBi at 8.5 GHz, 3.5 dBi at 27.9 GHz, 2.0 dBi at 37.1 GHz, 3.0 dBi at 66.5
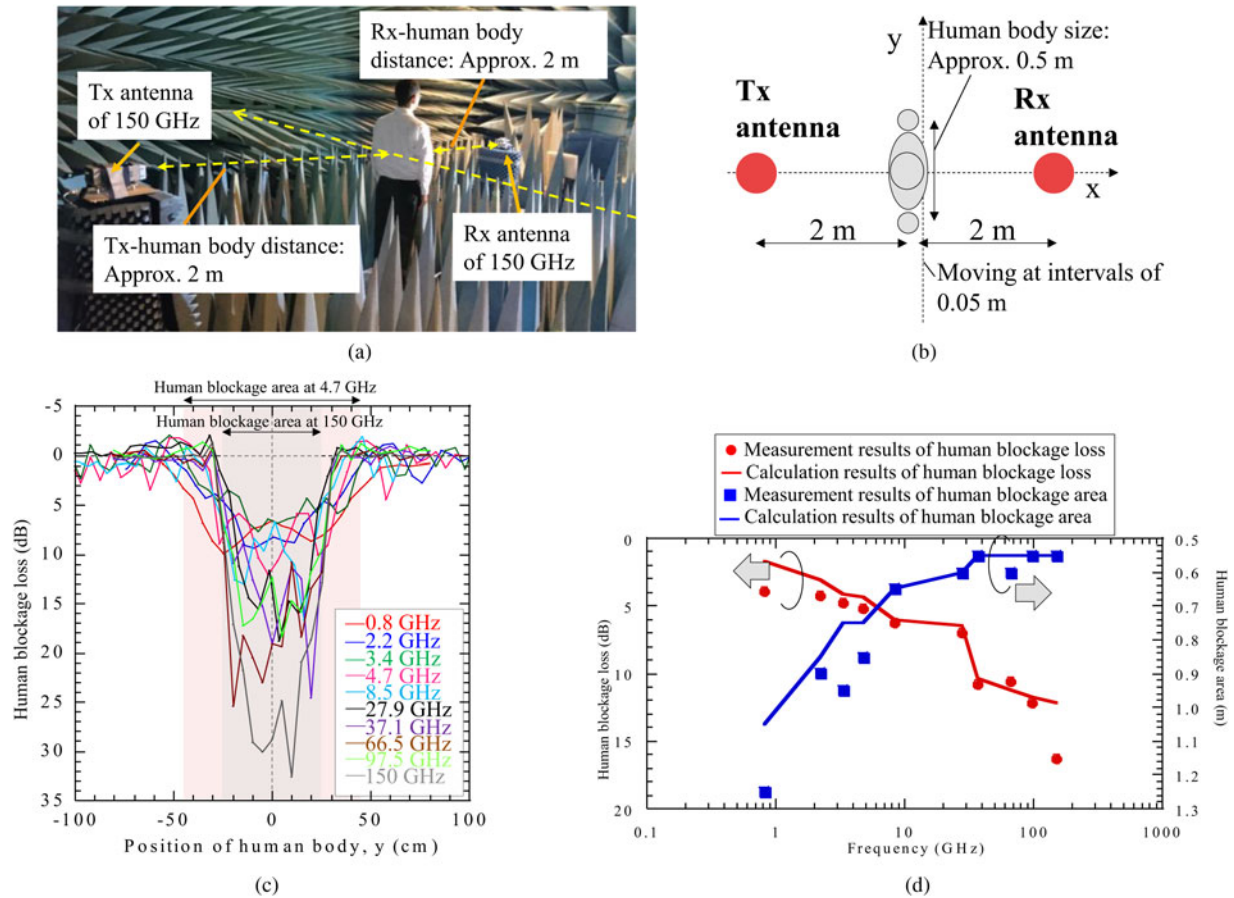
Fig. 3. Measurement setup and results. (a) Photo of anechoic chamber. (b) Top view of measurement setup. (c) Measurement of human blockage loss. (d) Comparison between measurement and calculation results using M.2412 human blockage model.

GHz, and 0 dBi at 97.5 GHz. At 150 GHz, the Tx and Rx antennas are a horn antenna with a beam width of 20° and an antenna gain of 23 dBi. Human blockage loss is calculated by subtracting the free-space path loss from the measurement path loss. The human blockage area is defined as the measured path loss that is larger than the free-space path loss due to the Fresnel zone shielding. In Fig. 3(c), the blockage area depends on frequency because as the Fresnel radius becomes small, the blockage area becomes small. Also, as the frequency increases, the human blockage loss increases. Figure 3(d) shows a comparison of the measurement and calculated results using the M.2412 human blockage model [4]. In that model, the human blockage loss is calculated by the knife-edge diffraction model using a finite width screen. In this paper, the diffraction loss is calculated by using a 0.5×1.7 m screen, which is the same as the measurement's human body size. Also, that model is constructed on the basis of the results equivalent to those using the omni-directional antenna. Since the angle required to radiate a human body from the Tx antenna is about 14°, it is narrower than the beam width of the Rx antenna at 150 GHz. Therefore, the obtained measurement of human blockage is equivalent to the results obtained using the omni-directional antenna. From these results, we find that the calculation results are similar to the measurement results, and the human blockage loss increases as the frequency increases, and the blockage area decreases as the frequency increases. The root mean square error (RMSE) of the loss is 1.6 dB. Therefore, the M.2412 human blockage model is valid to

evaluate the frequency dependency of human blockage loss up to the 150 GHz bands.

Scattering from rough surface

There is a trade-off between reflection and scattering from the rough surface shown in Fig. 4. The power of the incident wave is divided into the power of reflection and scattering from the rough surface, and the larger the scattering, the lower the reflection. Also, since roughness depends on the frequency, the higher the frequency, the larger the roughness. When the roughness is larger, the scattering is more significant. Therefore, the higher the frequency, the larger the roughness, the larger the scattering power, and the lower the reflection power. Therefore, it is necessary to clarify the relationship between reflected waves and scattered waves in the sub-THz bands. Figure 5 shows the measurement environment and setup. Scattering measurements from 2.2 to 97.5 GHz were conducted in front of a building's metal wall using the channel sounder summarized in Table 2. The Tx antenna is an omni-directional antenna with a beam width of about 60° at 2.2, 26.4, 66.5, and 97.5 GHz, and the Rx antennas are a Cassegrain antenna with a beam width of 2° at 66.5 and 97.5 GHz and 4° at 26.4 GHz, and a patch array antenna with a beam width of 8° at 2.2 GHz. The incident angle θ_i is set to 9° and the power delay profile (PDP) is measured at scattering angle θ_s from about −81° to 81° in 6° steps using the same clock frequency at the Tx and Rx equipments with an accuracy
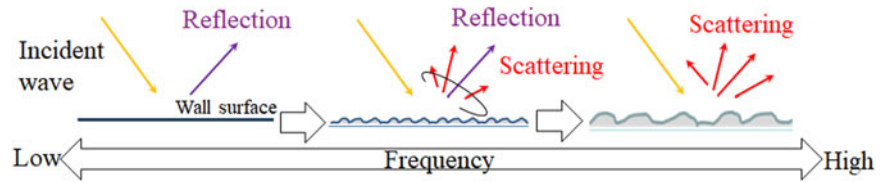
Fig. 4. Relationship between reflection and scattering. (a) Measurement building wall. (b) Measurement setup.
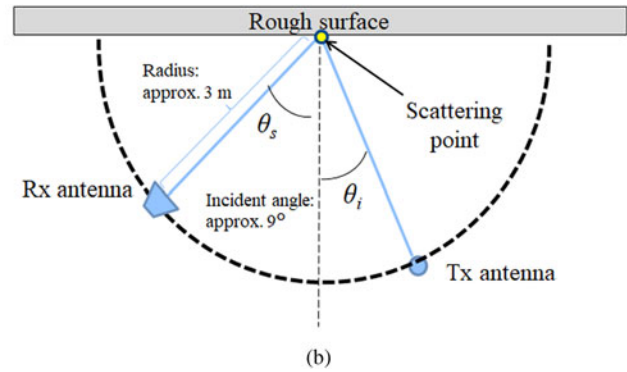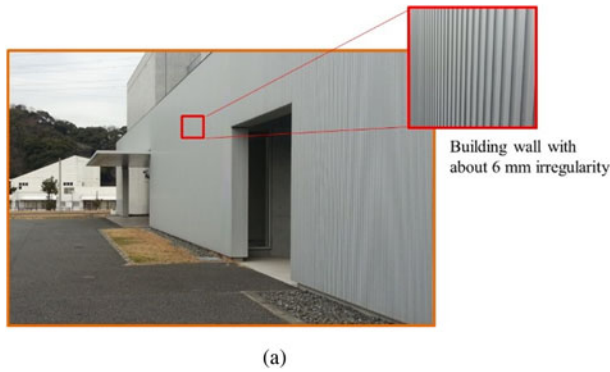
Fig. 5. Measurement environment and setup. (a) 97.5 GHz, (b) 66.5 GHz, (c) 26.4 GHz, (d) 2.2 GHz.

Table 2. Measurement parameters

Tx	Frequency	2.2, 26.4, 66.5, 97.5 GHz
	Bandwidth	50 MHz at 2.2 GHz, 100 MHz at 26.4 GHz, 500 MHz at 66.5 GHz, 97.5 GHz
	Modulation	OFDM at 97.5 GHz, BPSK at 26.4 GHz
	Antenna	Omni-directional antenna
	Antenna height	1.5 m
Rx	Antenna	Patch array antenna at 2.2 GHz, Cassegrain antenna at 26.4, 66.5, 97.5 GHz
	Antenna height	1.5 m

of about $\pm 1.0 \times 10^{-12}$. Calibration was performed so that the absolute value of the propagation delay distance could be obtained. The power of the path with the propagation delay distance of 6 m was defined as the scattering power, and that power was extracted from the PDP. Figure 6 shows the measured scattering patterns from the rough building surface. Scattering power is normalized by the peak value of the measured scattering power. As shown in Fig. 6, the scattered peak is observed at the specular reflection direction and the power tends to decrease as the scattering angle changes from the specular reflection direction. In addition, the scattering beam width which is defined as the width in the range 3 dB lower than the scattering peak becomes wider as the frequency increases (2.2 GHz: 10°, 26.4 GHz: 24°, 66.5 GHz: 60°, 97.5 GHz: 60°). Generally, the peak of angular profiles becomes wider as the beam width becomes wider. In addition, the measurement scattering peak for the higher frequency bands with a narrower beam width of the Rx antenna becomes wider than that for the lower frequency bands with a wider beam width. Therefore, the measurement results included the influence of the difference of Rx antenna beam width, but it is not the dominant factor. Next, we evaluated the frequency dependency of scattering by comparing the calculation

results using the effective roughness (ER) model with the measurement results. The ER model is widely used to predict the scattering. Although a number of scattering models and parameters have been reported [14], models and parameters need to be appropriately used on the basis of empirical or measurement results. Therefore, on the basis of measurement results, we calculated the scattering using a directive scattering (DS) model in which the scattering lobe is steered toward the direction of the specular reflection. The electric field E_s is defined as

$$|E_s|^2 = \left(\frac{K \cdot S}{r_i \cdot r_s}\right)^2 \cdot \frac{dS \cdot cos\theta_i}{F_\alpha}\left(\frac{1 + \cos \Psi_r}{2}\right)^\alpha \tag{1}$$

$$F_\alpha = \int\limits_0^{\pi/2}\int\limits_0^{2\pi}\left(\frac{1 + \cos \Psi_r}{2}\right)^\alpha \sin \theta_s d\theta_s d\varphi_s, \tag{2}$$

where F_α and α are constant values defining the scattering pattern and Ψ_r is the angle between the reflection direction and the scattering direction. As α becomes smaller, the scattering beam width becomes wider. K is a constant value depending on the amplitude of the impinging wave. θ_i is the incident angle, θ_s is the scattering angle, r_i is the incident vector, r_s is the scattering vector, and dS is the size of the surface elements. S is a scattering coefficient. In the simulation, the wall size was set to a 10×3 m screen. In the ER model's parameters, dS is set to 0.1 m. To investigate the frequency dependency of scattering, the scattering coefficient S and the coefficient related to the scattering beam width α are regressed on the basis of the measured scattering pattern within the main beam width. In Fig. 6, the blue line indicates the calculation results using the DS model. As shown in Figs 6(c) and 6(d), the discrepancy outside the main beam due to the effect of multi-path from the surrounding objects. However, the calculation results are similar to measurement results within the main beam. The RMSE within the main
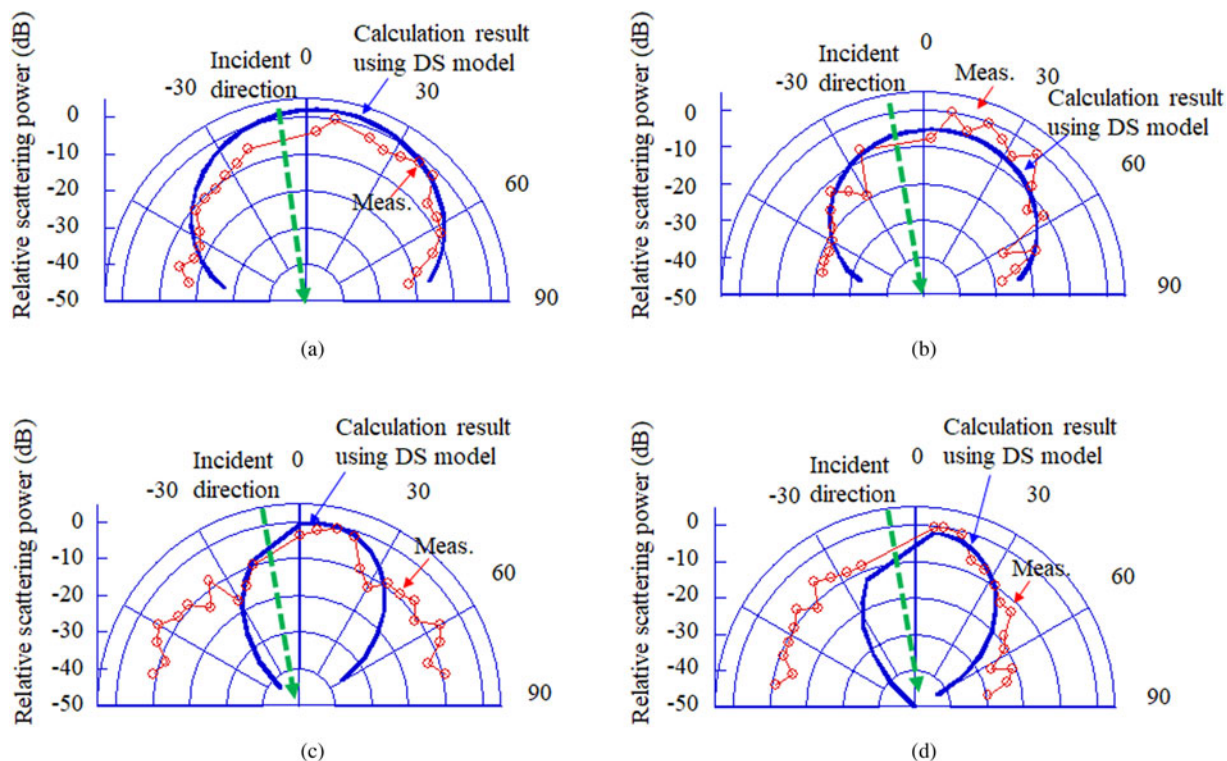
Fig. 6. Frequency dependency of scattering from rough building surface.
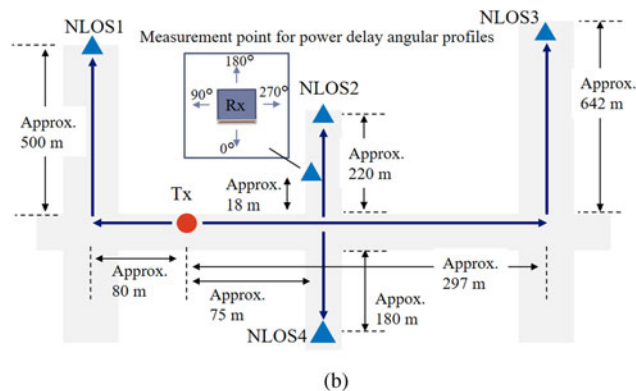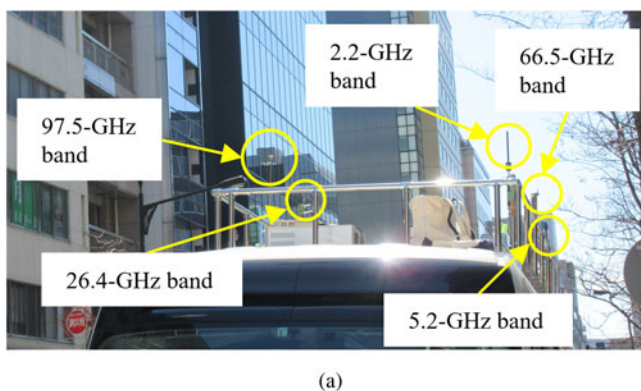
Fig. 7. Measurement setup. (a) Configuration of Tx antenna. (b) Measurement routes.

beam is about 4.7, 2.3, 3.2, and 4.2 dB at 2.2, 26.4, 66.5, and 97.5 GHz, respectively. Therefore, the scattering from the rough surface is the dominant path within the main beam. The regression results are $S = 0.7$ and $\alpha = 40$ at 2.2 GHz, $S = 0.6$ and $\alpha = 40$ at 26.4 GHz, $S = 0.7$ and $\alpha = 10$ at 66.5 GHz, and $S = 0.6$ and $\alpha = 10$ at 97.5 GHz. This indicates that the scattering beam widths at 66.5 and 97.5 GHz are wider than 2.2 and 26.4 GHz, respectively. In this environment, the wavelengths at 2.2 and 26.4 GHz were longer than the irregularity of the building wall, which is about 6 mm. In contrast, the wavelengths at 66.5 and 97.5 GHz were shorter. Therefore, the scattering is considered to have been more diffused in the 66.5 and 97.5 GHz bands. Since buildings in an urban environment have various irregularities and rough surfaces, scattering due to them could be more diffused than in this environment and affect the path-loss characteristics.

UMi path-loss characteristics

The path-loss measurement environment around Tokyo Station, Japan is shown in Fig. 7. The measurement parameters are summarized in Table 3. The frequencies for measuring frequency dependency were from 2.2 to 97.5 GHz. The Tx used these frequencies to transmit CW signals, and the Rx measured the path loss at those frequencies while moving along the measurement routes NLOS1, NLOS2, NLOS3, and NLOS4. The M.2412 path-loss models were compared with the results of regression using the measurement data [4]. In the LOS environment of M.2412, the path-loss coefficient n was obtained by regressing the measured path loss to the single-frequency close-in (CI) free-space reference distance model, as expressed by equation (3).

$$PL_{CI} = 10n \log_{10}(d_{3D}) + FSPL(f_c, 1\,\text{m}) \tag{3}$$

Table 3. Parameters used in measurement path loss and power angular profiles

Parameters for path loss	Frequency	2.2, 5.2, 26.4, 66.5, 97.5 GHz
	Signal	CW
	Tx/Rx antenna	Omni-directional antenna
	Tx/Rx antenna height	3.3/2.6 m
Parameters for power angular profiles	Frequency	26.4, 97.5 GHz
	Modulation	BPSK at 26.4 GHz, OFDM at 97.5 GHz
	Bandwidth	100 MHz at 26.4 GHz, 500 MHz at 97.5 GHz
	Tx/Rx antenna	Omni-directional antenna/Cassegrain antenna
	Tx/Rx antenna height	3.3/1.5 m
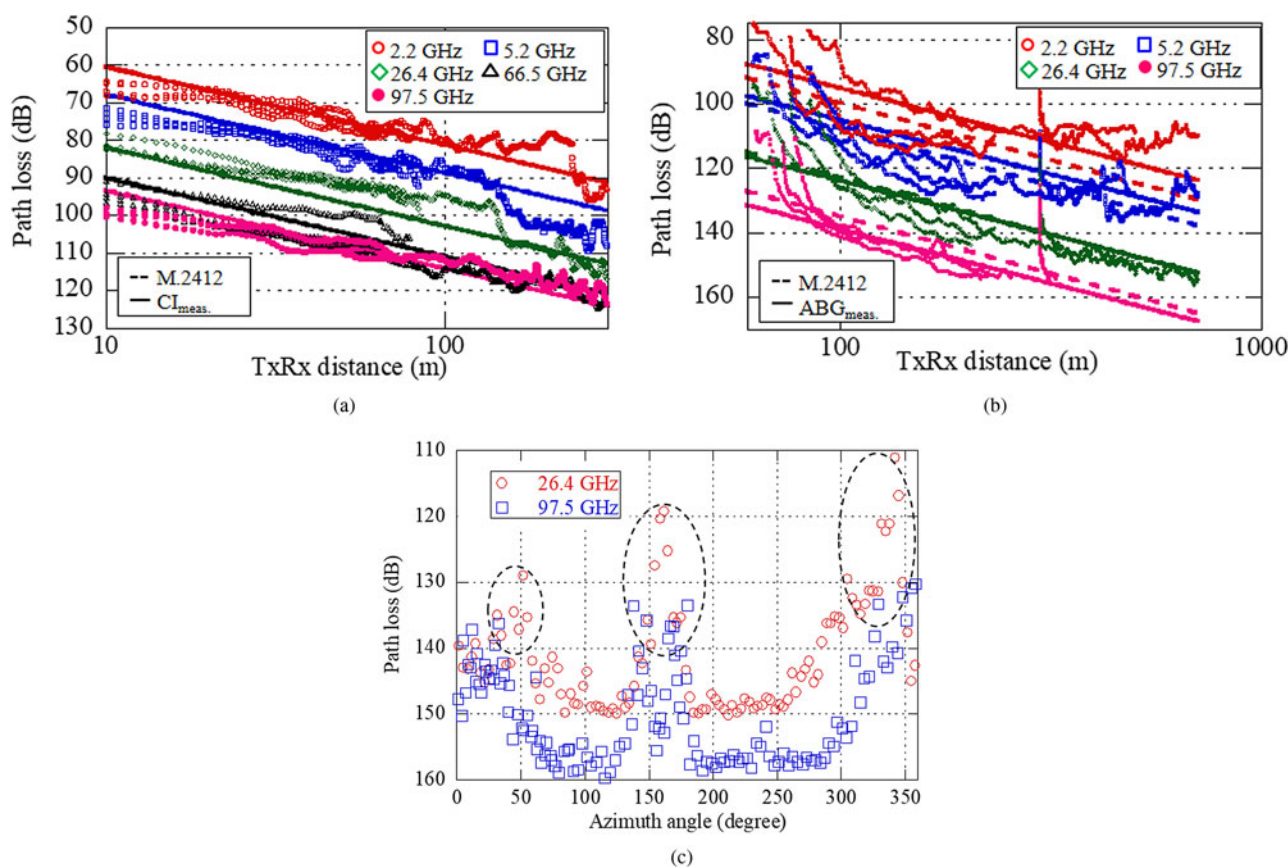
Fig. 8. Measurement results. (a) Path-loss characteristics in LOS environment. (b) Path-loss characteristics in NLOS environment. (c) Measured power angular profiles.

$$FSPL(f_c, d_{3D}) = 32.4 + 20\log_{10}(f_c) + 20\log_{10}(d_{3D}), \quad (4)$$

where d_{3D} is Tx-Rx distance and f_c denotes the frequency. In contrast, in the NLOS environment of M.2412, parameters α, β, and γ were obtained by regressing the measured path loss to the alpha-beta-gamma (ABG) model, as expressed by equation (5).

$$PL_{ABG} = 10\alpha\log_{10}(d_{3D}) + \beta + 10\gamma\log_{10}(f_c). \quad (5)$$

Path-loss characteristics are shown in Figs 8(a) and 8(b), and the coefficient values of the M.2412 path-loss models and the

results of regression using the measured path loss are compared in Table 4. From Fig. 8(a) in the LOS environment, the path loss calculated using the M.2412 path-loss model shows a similar trend to the measured path loss, and the RMSE is 4.0 dB. According to Table 4, the path-loss coefficient n is the same value in the case of the M.2412 path-loss model. This result confirms that in the LOS environment, the M.2412 path-loss model is valid from 2.2 to 97.5 GHz. It is clear from Table 4 in NLOS environment that the results of regression using equation (5) ABG_{meas} show better prediction accuracy than the path loss calculated using the M.2412 path-loss model. A possible

Table 4. Comparison results

		n	Constant loss (dB)		RMSE (dB)
LOS	CI_{meas}	2.1	$32.4 + 20\log_{10} f_{GHz}$		4.0
	M.2412	2.1	$32.4 + 20\log_{10} f_{GHz}$		4.0
		α	β (dB)	γ	RMSE (dB)
NLOS	ABG_{meas}	3.36	19.0	2.65	7.2
	M.2412	3.53	22.0	2.13	8.1

factor for error is that coefficient γ related to frequency dependency is larger than that of the M.2412 path-loss model. These results indicate that the frequency dependency of the measured path loss is stronger than that of M.2412 path-loss model. Therefore, we analyzed the measured power angular profiles (PAPs), and we clarified the factors that affect path-loss frequency dependency. PAPs were measured along NLOS2. The measurement parameters are summarized in Table 3. The PDPs at 26.4 and 97.5 GHz were measured while the Cassegrain antenna was rotated 360 degrees in the azimuth plane and 0–60 degrees in the elevation plane along NLOS2. The Rx antenna was a Cassegrain antenna with a beam width of 2° at 97.5 GHz and 4° at 26.4 GHz. In the post-processing, maximum received power in the PDP was extracted first, and maximum received power elevation angles from 0 to 60 degree was extracted next, and PAPs in the azimuth plane were obtained. The measured PAPs at 26.4 and 97.5 GHz along NLOS2 are shown in Fig. 8(c). Three dominant arrival paths were measured at 26.4 and 97.5 GHz from surrounding buildings and structures. The summation result of path loss of those three dominant paths at 26.4 GHz is about 109 dB and that at 97.5 GHz is about 129 dB and the difference is 20 dB. Since the difference expressed by the Friis FSPL equation for 26.4 and 97.5 GHz is $20\log_{10}(97.5/26.4\,\text{GHz}) \fallingdotseq 11.4$ dB, the frequency dependency is about 8.6 dB larger than that given by the Friis FSPL equation. In an UMi environment, it is assumed that the higher the frequency, the scattering is more diffused, and the reflection power of the arrival paths at 97.5 GHz could be decreased compared with that at 26.4 GHz.

Conclusion

In this paper, we showed the investigation results of frequency dependency of human blockage, scattering effects from a rough building surface, and path-loss characteristics in an UMi up to 150 GHz. Human blockage loss increases as the frequency increases and a representative M.2412 model could evaluate the frequency dependency of human blockage loss up to 150 GHz bands. To evaluate scattering from a rough building surface, it is confirmed that the scattering from a rough surface is considered to be more diffused in the 66.5 and 97.5 GHz bands than in the 2.2 and 26.4 GHz bands. In the path-loss characteristics in UMi, a comparison of measured path loss and M.2412 path-loss models showed that the M.2412 path-loss model is valid in LOS environment. In contrast, in the NLOS environment, it was found that path-loss frequency dependency is stronger than that given by the M.2412 path-loss model. In addition, the measured PAPs indicate that reflection waves from the surrounding buildings and structures are the dominant paths in NLOS environment and the path-loss frequency dependency increases as the power

of reflection waves decreases. By utilizing these characteristics for the radio propagation simulation, we believed that the accuracy of the new 6G radio-network topology design for sub-THz bands can be improved.

References

1. **WRC2019**. WRC 2019 agenda item details.
2. **NTT DOCOMO, INC** (2020). White paper, 5G evolution and 6G.
3. **FCC News Release** (2019) FCC takes steps to open spectrum horizons for new services and technologies.
4. **Rep. ITU-R M.2412-0** (2017) Guidelines for evaluation of radio interface technologies for IMT-2020.
5. **METIS** (2015) Deliverable D1.4, METIS channel models.
6. **MiWEBA** (2014) Channel modeling and characterization, *Deliverable D5.1.*
7. **Aalto University, Nokia, AT&T, NTT DOCOMO, BUPT, New York University, CMCC, Qualcomm, Ericsson, Samsung, Huawei, University of Bristol, INTEL, University of Southern California, KT Corporation** (2016) White paper on 5G channel model for bands up to 100 GHz, Global Communications Conference (GLOBECOM), 3rd Workshop on Mobile Communications in Higher Frequency Bands, Washington DC, U.S.A.
8. **Inomata Minoru, Yamada Wataru, Kuno Nobuaki, Sasaki Motoharu, Kitao Koshiro, Nakamura Mitsuki, Ishikawa Hironori and Oda Yasuhiro** (2021) Terahertz propagation characteristics for 6G mobile communication systems, 2021 15th European Conference on Antennas and Propagation (EuCAP), pp. 1–5.
9. **Teyeb Oumer, Muhammad Ajmal, Mildh Gunnar, Dahlman Erik, Barac Filip and Makki Behrooz** (2019) Integrated access backhauled networks, IEEE VTC2019-Fall, pp. 1–5.
10. **Kitayama Daisuke, Hama Yuto, Goto Kenta, Miyachi Kensuke, Motegi Takeshi and Kagaya Osamu** (2021) Transparent dynamic metasurface for a visually unaffected reconfigurable intelligent surface: controlling transmission/reflection and making a window into an RF lens. *Optics Express* **29**(18), 29292–29307.
11. **Rec. ITU-R P.676-12** (2019) Attenuation by atmospheric gases and related effects.
12. **Rec. ITU-R P.838-3** (2005) Specific attenuation model for rain for use in prediction methods.
13. **Rec. ITU-R P.833-9** (2016) Attenuation in vegetation.
14. **Degli-Esposti Vittorio, Fuschini Franco, Vitucci M. Enrico and Falciasecca Gabriele** (2007) Measurement and modelling of scattering from buildings. *Transactions on Antennas and Propagation IEEE* **55**, 143–152.

Minoru Inomata received his B.E. and M.E. degrees in electrical engineering from Tokyo University of Science and his Ph.D. degree from Tokyo Institute of Technology, Japan, in 2009, 2011, and 2019, respectively. Since joining NTT in 2011, he has been engaged in research of radio propagation for 6G, 5G, and unlicensed wireless communication systems.

Wataru Yamada received his B.E., M.E., and Ph.D. degrees from Hokkaido University, Japan, in 2000, 2002, and 2010, respectively. Since joining NTT in 2002, he has been engaged in research of propagation characteristics for wideband access systems. He is currently a Distinguished Researcher in NTT Access Network Service Systems Laboratories.

Nobuaki Kuno received his B.E. and M.E. degrees from the University of Electro-Communications, Tokyo, Japan in 2014 and 2016, respectively. He joined NTT Access Network Service Systems Laboratories in 2016. He has been engaged in research of machine learning for radio propagation modeling.

Motoharu Sasaki received his B.E. degree in engineering and his M.E. and Ph.D. degrees from Kyushu University, Japan in 2007, 2009, and 2015, respectively. In 2009, he joined NTT Access Network Service Systems Laboratories, Japan. He has been engaged in research on propagation modeling.

Koshiro Kitao received his B.S., M.S., and Ph.D. degrees from Tottori University, Tottori, Japan in 1994, 1996, and 2009 respectively. He joined the Wireless Systems Laboratories, NTT, Japan in 1996. Since then, he has been engaged in research of radio propagation for mobile communications. He is now an Assistant Manager of the 6G-IOWN Promotion Department, NTT DOCOMO, INC., Japan.

Mitsuki Nakamura received his B.E. and M.E. degrees from Keio University, Tokyo, Japan in 2012 and 2014, respectively. He joined NTT Access Network Service Systems Laboratories in 2014. He has been engaged in research of radio propagation characteristics and radio propagation for wireless access systems. He is now a member of the 6G-IOWN Promotion Department, NTT DOCOMO, INC.

Takahiro Tomie received his B.S., M.S., and Ph.D. degrees from Tohoku University, Japan in 2005, 2007, and 2010, respectively. He joined the Research Laboratories, NTT DOCOMO, INC., Japan in 2010. Since then, he has been engaged in research of radio propagation for mobile communications.

Yasuhiro Oda received his B.S. degree from Nagoya University, Nagoya, Japan in 1990. He joined NTT Laboratories, Japan in 1990. Since then, he has been engaged in research and development of cellular systems and radio propagation. He is now a senior manager in the 6G-IOWN Promotion Department, NTT DOCOMO, INC.